PAPER

Self-assembly-based photonic crystal slabs for refractive index sensing via bound states in the continuum

IOP Publishing Journal of Optics
J. Opt. **27** (2025) 115102 (7pp) https://doi.org/10.1088/2040-8986/ae19f9

Self-assembly-based photonic crystal slabs for refractive index sensing via bound states in the continuum

Yuyang Xu[1,2,5], **Shunben Wu**[1,2,5], **Ang Jiang**[1,2,5], **Xiaohan Liu**[1,2], **Jiajun Wang**[1,2,*] and **Lei Shi**[1,2,3,4,*]

[1] Shanghai Research Center for Quantum Sciences, Shanghai 201315, People's Republic of China
[2] State Key Laboratory of Surface Physics, Key Laboratory of Micro- and Nano-Photonic Structures (Ministry of Education) and Department of Physics, Fudan University, Shanghai 200433, People's Republic of China
[3] Institute for Nanoelectronic Devices and Quantum Computing, Fudan University, Shanghai 200438, People's Republic of China
[4] Collaborative Innovation Center of Advanced Microstructures, Nanjing University, Nanjing 210093, People's Republic of China

E-mail: jiajunwang@fudan.edu.cn and lshi@fudan.edu.cn

Received 7 August 2025, revised 18 September 2025
Accepted for publication 31 October 2025
Published 13 November 2025

Abstract

Bound states in the continuum (BICs) have drawn extensive attention in optics and photonics due to their ultrahigh quality (Q) factors, which make them ideal for high-sensitivity sensing applications. Existing approaches to realize BIC-supporting nanostructures in the optical regime often rely on expensive and complex fabrication methods such as electron beam lithography. Here, we propose a self-assembly-based method to fabricate photonic crystal (PhC) slabs working in the optical regime. In the fabricated PhC slab, the symmetry-protected BIC was directly observed. By integrating the PhC slab into a microfluidic chip, we characterized the related quasi-BIC mode and demonstrated its sensing performance in various concentrations of NaCl solutions, achieving a sensitivity of 110 nm/RIU.

Keywords: bound state in the continuum, photonic crystal slabs, self-assembly micro-spheres arrays, refractive index sensing

1. Introduction

Refractive index (RI) sensing plays a crucial role in a wide range of applications, including medical diagnostics [1, 2], environmental monitoring [3, 4], and chemical analysis [5, 6]. A commonly employed strategy for optical RI sensing involves the use of nanophotonic structures to support optical resonances, where slight shifts in the resonant modes can indicate changes in the surrounding RI. Over the past years, a variety of resonant nanophotonic platforms, particularly those based on plasmonic and dielectric resonances, have been extensively investigated for this purpose [1, 7–16]. In these platforms, resonances with a high quality factor (Q factor) are particularly desirable, as they generally provide higher sensitivity in RI sensing.

More recently, bound states in the continuum (BICs) supported in photonic crystal (PhC) slabs have attracted attention in optics and photonics due to their ultrahigh Q factors, which make them ideal for high-sensitivity RI sensing [17–19]. As non-radiative states with infinite Q factors, BICs are not accessible in far-field measurements and thus unavailable for direct sensing applications. Hence, radiative high-Q modes related to BICs are actually required in practical RI sensing

[5] Authors contributed equally to this paper.
[*] Authors to whom any correspondence should be addressed.

applications. On the one hand, by breaking the symmetry of the PhC slabs, high-Q modes can evolve from the original BICs. On the other hand, without breaking any symmetry, the optical modes with high-Q naturally exist near the BICs. These high-Q modes, referred to as quasi-BICs, have been extensively explored for RI sensing using nanophotonic structures [19–33].

For the fabrication of PhC slabs that support BICs in the optical regime, electron beam lithography (EBL) processes are typically required due to their ability to realize highly precise, customized nano-photonic structures. Yet, this method still faces challenges, such as the need for costly and sophisticated equipment and their time-consuming nature. To address these challenges, it is important to explore different fabrication strategies. The microsphere self-assembly method is widely regarded as a low-cost and convenient approach for fabricating periodic nanophotonic structures, such as PhC slabs [34–36]. In addition to direct use, self-assembled patterns can also serve as masks for subsequent etching processes, enabling the fabrication of a broader variety of PhC slabs [35–37]. In recent years, PhC slabs fabricated via self-assembly have been extensively applied in diverse areas and have also shown potential for sensing applications [38–43]. However, to date, the use of self-assembly-based PhC slabs to realize BICs for RI sensing remains unexplored.

In this work, we demonstrate a self-assembly-based PhC slab that supports BICs for RI sensing. The PhC slab consists of a hexagonal lattice of silicon nitride cylinders on a silica substrate, supporting symmetry-protected BICs at the Γ point. Near the BICs, quasi-BIC modes with high Q factors exist and appear as resonance peaks in the reflection spectra. The resonance peaks shift in response to changes in the surrounding RI, enabling RI sensing. This PhC slab was fabricated by using a self-assembled polystyrene (PS) microsphere array as a mask, followed by reactive ion etching (RIE) to form silicon nitride cylinders. By integrating the fabricated PhC slab into a microfluidic chip, both the BIC and quasi-BIC modes were characterized in the angle-resolved reflection spectra. Using NaCl solutions of varying concentrations, the shift in a quasi-BIC mode was observed, showing a sensing sensitivity of 110 nm/RIU.

2. Design and simulation

Figure 1 shows the schematic of RI sensing using a PhC slab made of Si_3N_4 cylinders on the SiO_2 substrate. The PhC slab is surrounded by a liquid environment, where the RI is denoted as n. To sense the RI of surrounding liquid, the PhC slab is illuminated at an incident angle of θ. When θ is small, the reflection spectra show peaks originating from resonances of quasi-BIC modes. The positions of these peaks shift as the RI of the surrounding liquid changes. By measuring the peak positions in the spectra, the corresponding RI can be determined, thereby realizing RI sensing.

To start, we designed a PhC slab for RI sensing via BICs, as shown in figure 2(a). It has a hexagonal lattice structure

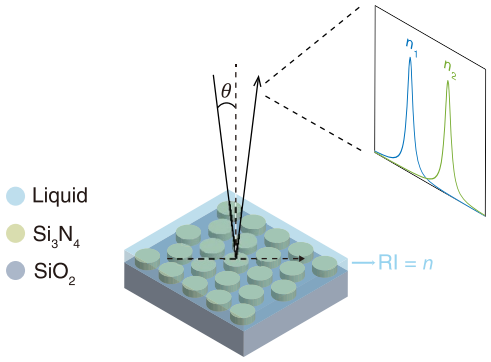

Figure 1. Schematic view of refractive index (RI) sensing using a photonic crystal (PhC) slab. The PhC slab is surrounded by a liquid environment with RI denoted as n and is illuminated at an incident angle θ. The reflection spectra show peaks originating from resonances of quasi-BIC modes. The peak positions shift with the surrounding RI, enabling RI sensing.

with period $a = 600$ nm and the diameter of cylinders $d = 450$ nm. The height of the cylinders is 150 nm. Two high-symmetry directions of the hexagonal lattice structure, $\Gamma - M$ and $\Gamma -$ K, are marked on the lattice. The eigenmodes of this PhC slab along the $\Gamma - M$ and $\Gamma - K$ directions were simulated using the finite element method. In the simulation, the surrounding RI is set to $n = 1.33$ to simulate a water environment. Figure 2(b) shows the simulated band structure together with the corresponding quality (Q) factors. The horizontal axis represents the angle associated with the in-plane momentum of the modes. A BIC mode exists at the Γ point, as denoted by the green dot, and a related quasi-BIC mode located at 3° along the $\Gamma - K$ direction is denoted by the blue dot. Figure 2(c) shows the simulated electric field amplitude distributions of these two modes. They display similar near-field distributions. Figure 2(d) shows the distributions of corresponding E_x components for both modes. We can see that the BIC mode is non-radiative, while the quasi-BIC mode leaks into plane waves, with a Q factor of 990. This makes the quasi-BIC mode accessible in far-field measurements.

To demonstrate the optical response of these modes, we simulated the angle-resolved reflection spectra of the PhC slab, using rigorous coupled-wave analysis. Typically, due to the presence of direct reflection, the reflection spectra exhibit Fano-shaped peaks [44], which can complicate the analysis of resonance peak positions. To suppress such non-resonant background signals, the cross-polarization setting is employed, a method that has been applied in various studies, including beam shift measurements and vortex beam generation [45, 46]. In the cross-polarization setting, direct reflection signals that preserve the incident polarization are suppressed, and the spectra primarily originate from the response of resonant modes themselves, manifesting as Lorentzian-shaped peaks [47]. In this simulation, the polarizations of incident and reflected light are set to $|+45\rangle = \frac{1}{\sqrt{2}}(|s\rangle + |p\rangle)$ and $|-45\rangle = \frac{1}{\sqrt{2}}(|s\rangle - |p\rangle)$, respectively. Here, $|s\rangle$ and $|p\rangle$ are linear polarizations perpendicular and parallel to the plane of incidence, defined with respect to the

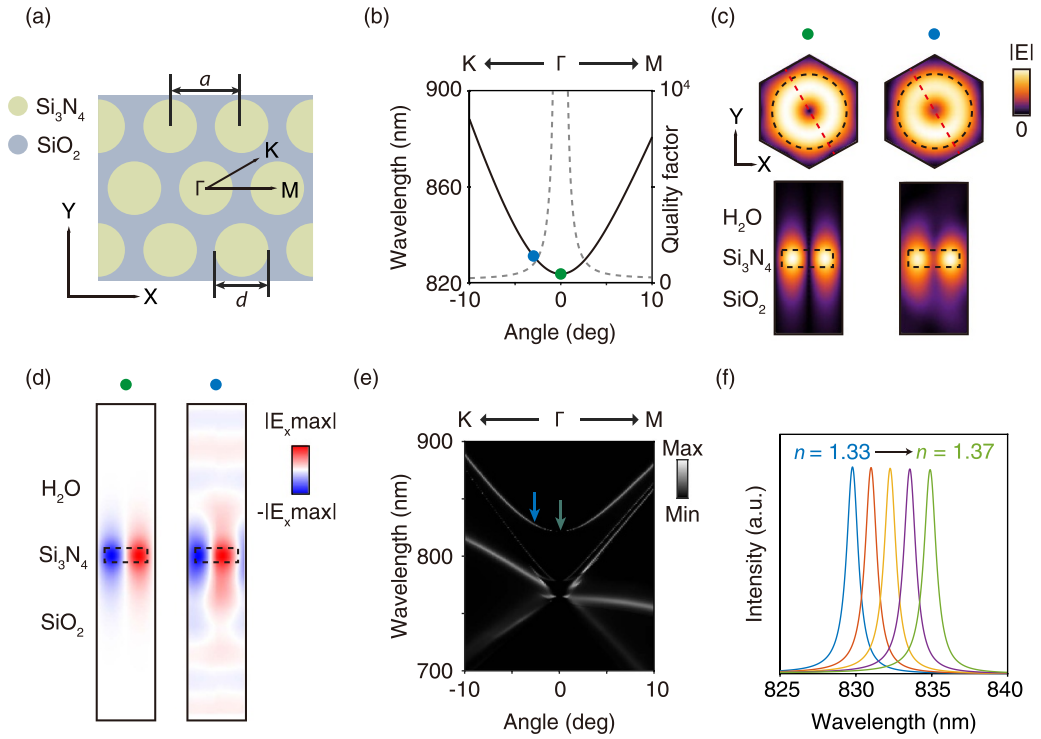

Figure 2. Sample design and simulations. (a) Schematic of the hexagonal lattice structure of the PhC slab. The PhC slab consists of Si_3N_4 cylinders on a SiO_2 substrate, with period a and cylinder diameter d. $\Gamma - M$ and $\Gamma - K$ denote two high symmetry directions in the lattice. (b) Simulated band structure (solid line) together with the corresponding quality (Q) factors (dashed line) of the eigenmodes of the PhC slab with surrounding RI $n = 1.33$. The horizontal axis represents the angle associated with the in-plane momentum of the modes. Green dot: BIC mode; Blue dot: quasi-BIC mode. (c) Simulated electric field amplitude distributions of the modes marked in (b). The black dashed lines depict the boundaries of the Si_3N_4 cylinders. Upper panel: XY cross-section at half the height of the Si_3N_4 cylinders. Lower panel: vertical cross-section along the red dashed lines marked in the upper panel. (d) Simulated distributions of E_x components of the modes marked in (b). The cross-section is taken along the same plane as in the lower panel of (c). (e) Simulated angle-resolved reflection spectra of the PhC slab with surrounding RI $n = 1.33$ under the cross-polarization setting. The green arrow at 0° indicates a BIC, and the blue arrow at 3° indicates the quasi-BIC mode. (f) Reflection spectra of the quasi-BIC mode marked by the blue arrow in (e) for different surrounding refractive indices, ranging from 1.33 to 1.37, in steps of 0.01.

incident light's wave vector. Moreover, $|s\rangle$ and $|p\rangle$ are also eigenpolarizations of the modes along the $\Gamma - \mathrm{M}$ and $\Gamma - \mathrm{K}$ directions, which are protected by the mirror-symmetry. The resulting reflection spectra are shown in figure 2(e). The resonant modes manifest as peaks in the spectra, and a non-radiative BIC remains dark, as marked by the green arrow. The quasi-BIC mode at 3° along the $\Gamma - \mathrm{K}$ direction is marked by the blue arrow. To simulate the sensing performance of this mode, we calculated the spectra at the fixed incident angle of 3° under varying surrounding RI, ranging from 1.33 to 1.37 in steps of 0.01. The results are shown in figure 2(f). A linear shift of the peak positions is observed with changes in the surrounding RI. The corresponding sensing sensitivity can be calculated by $S = \Delta\lambda/\Delta n$, where Δn represents the change in the surrounding RI, and $\Delta\lambda$ represents the corresponding wavelength shift of the peak position. It shows a high sensitivity of 127.8nm/RIU (RIU: refractive index unit).

3. Results and discussions

The designed PhC slab was fabricated based on the microsphere self-assembly method. The fabrication process is shown in figures 3(a)–(d). First, a monolayer of closely packed PS microspheres is self-assembled onto a Si_3N_4 film deposited on a SiO_2 substrate (figure 3(a)). Here, the diameter of PS microspheres corresponds to the period a of the structure. Next, oxygen RIE is applied to reduce the diameter of the PS microspheres (figure 3(b)). These etched microspheres then serve as a mask for patterning the Si_3N_4 film into cylinders via RIE with CHF_3 and O_2 (figure 3(c)). The diameter of the cylinders d is determined by the size of the microspheres in the mask. Finally, the microsphere mask is removed by RIE with O_2, completing the fabrication of the PhC slab (figure 3(d)). From the scanning electron micrographs, we can see that the fabricated structure is consistent with our design.

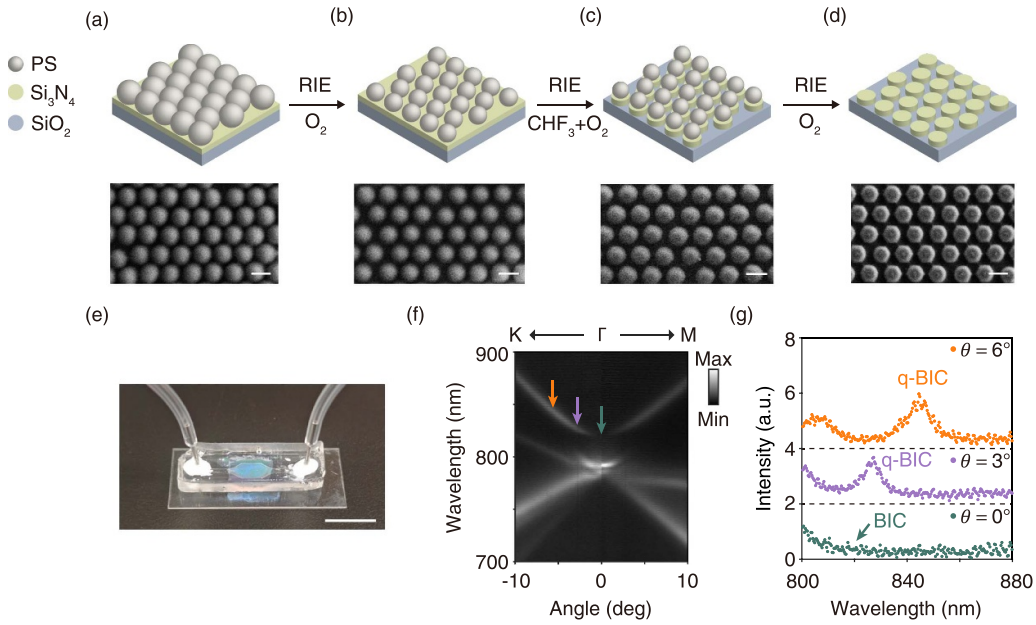

Figure 3. Sample fabrication and characterization. (a)–(d) Fabrication process of the PhC slab. Upper panels: schematic illustrations. Lower panels: scanning electron micrographs. Scale bar: 500 nm. (e) Photograph of the microfluidic chip incorporating the fabricated PhC slab for RI sensing. Scale bar: 1 cm. (f) Measured angle-resolved reflection spectra of the PhC slab in water. The polarization setup is the same as in figure 2(e). (g) Reflection spectra extracted from (f) at incident angles $\theta = 0°$, $3°$ and $6°$ along $\Gamma - \mathrm{K}$ direction.

To enable measurements in a liquid environment, the fabricated PhC slab was integrated into a microfluidic chip made of polydimethylsiloxane, as shown in figure 3(e). We then measured the angle-resolved reflection spectra of the PhC slab using a homemade momentum-space imaging spectroscopy based on the Fourier optics [17, 48], with the same polarization setup as in the simulation. The spectra measured in a water environment are presented in figure 3(f). We can see the measured spectra agree well with the simulation in figure 2(e). The spectra at $0°$, $3°$ and $6°$ along $\Gamma - \mathrm{K}$ direction were extracted and are plotted in figure 3(g). At the Γ point ($0°$), a BIC exists, which corresponds to the absence of a resonance peak in the spectrum. At small deviations from the Γ point ($3°$ and $6°$), resonance peaks appear in the spectra, corresponding to quasi-BIC modes. The resonance peak at $3°$ is narrower, indicating a higher Q factor of the mode compared to that at $6°$, making it a suitable candidate for RI sensing.

To demonstrate the sensing performance of the fabricated PhC slab, we measured the reflection spectra at $3°$ under NaCl solutions with different mass fractions of NaCl (ω). Figures 4(a)–(c) show the spectra measured at $\omega = 0\%$, 2%, and 4%, respectively. Each spectrum is obtained by averaging five repeated intensity measurements. At each mass fraction, the resonance peak exhibits the characteristics of a Lorentzian line shape. To extract the resonance peak centers of the spectra, a Lorentzian fit was performed, over the range from 815 nm to 840 nm. The solid lines in figures 4(a)–(c) represent the fitted curves. The fitted peak centers for each ω are marked in the figures, and a clear shift in the peak center is observed as ω varies, reflecting the corresponding RI changes in the solutions. To demonstrate the stability of our measurements, we also calculated the standard deviation from three repeated spectra measured at $\omega = 0\%$, and found it to be 0.076 nm, which is much smaller than the observed peak shifts. In addition, the full width at half maximum obtained from the Lorentzian fit is about 8 nm, from which the corresponding quality factor of the mode can be estimated as 103. Figure 4(d) summarizes the fitted peak centers with ω ranging from 0% to 18%, in steps of 2%. The error bars represent the standard deviations from the Lorentzian fit, which are about 0.1 nm. The results show a good linear relationship between the peak center and the mass fraction of NaCl. The slope obtained from the linear fit indicates the sensing sensitivity. Considering that a change of $\Delta\omega = 0.01$ approximately corresponds to a RI change of 0.0017 RIU [49], it shows a sensitivity of $S = 110\,\mathrm{nm/RIU}$. This demonstrates a reliable RI sensing performance of the PhC slab, as intended in the design.

Next, we compare our results with previously reported works to place them in the context, as shown in table 1. The RI sensor proposed in this work achieves a sensitivity comparable to those reported for other quasi-BIC-based sensors, while employing self-assembly method rather than EBL for fabrication. Despite some limitations in pattern flexibility and fabrication precision, the self-assembly method still provides reliable performance suitable for typical sensing applications. Compared with EBL, a commonly used but expensive method for precisely creating customized nano-photonic structures, the self-assembly method offers advantages in terms of cost-effectiveness and convenience, which could facilitate practical sensing applications.

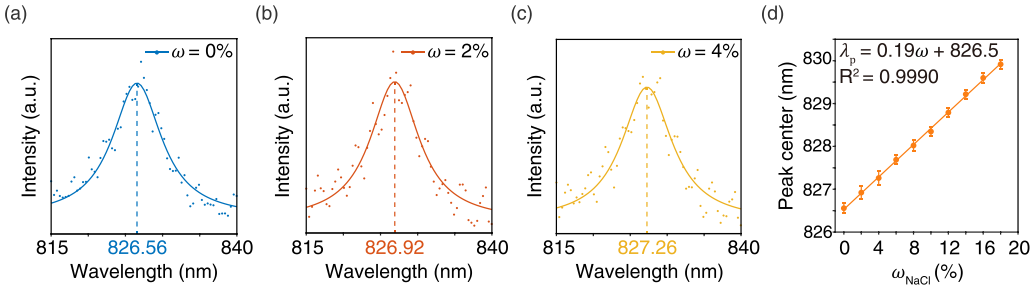

Figure 4. RI sensing. (a)–(c) Reflection spectra of quasi-BIC modes in NaCl solutions with NaCl mass fractions $\omega = 0\%$, 2%, and 4%, respectively. Dots: measured intensities. Solid lines: Lorentzian fits. Dashed lines: peak centers of the fits. (d) Peak centers of quasi-BIC modes at various NaCl concentrations. Dots: fitted peak centers. Error bars: standard deviations from Lorentzian fitting. Line: linear fit.

Table 1. Comparison of RI sensors via quasi-BICs in recent works. EBL: electron beam lithography.

Reference	Structure	Fabrication method	Operating wavelength (nm)	Sensitivity (nm/RIU)
Photonics Research, 6(7):726–733, 2018. [20]	Si_3N_4 photonic crystal slab	EBL	785	178
Advanced Functional Materials, 31(46):2104 652, 2021. [23]	Si crescent metasurface	EBL	660	326
Optics Express, 27(13): 18 776–18 786, 2019. [30]	Si_3N_4 photonic crystal slab	EBL	540	103
IEEE Photonics Journal, 12(5):1–10, 2020. [31]	Si photonic crystal slab	EBL	1563	36
ACS Nano, 18(8):6477–6486, 2024. [32]	Si_3N_4 hybrid metasurface	EBL	760, 870	493, 312
Nanophotonics, 13(4):463–475, 2024. [33]	Si dual nanorod metasurface	EBL	1530, 1620	408, 236
This work	Si_3N_4 photonic crystal slab	Self-assembly	830	110

4. Conclusion

In conclusion, we propose a PhC slab based on a self-assembly fabrication process for RI sensing via BICs. Employing the microsphere self-assembly method, the PhC slab can be fabricated cost-effectively and conveniently. The PhC slab enables RI sensing through shifts in the resonance peaks of quasi-BIC modes in the reflection spectra. We fabricated the PhC slab and experimentally characterized both the BIC and quasi-BIC modes. Under different concentrations of NaCl solutions, a clear shift in the resonance peaks of quasi-BIC modes is demonstrated, and it exhibits a sensing sensitivity of 110 nm/RIU. The proposed PhC slab, combining a practical and cost-effective fabrication method with high sensing performance, highlights the potential of quasi-BIC modes for advanced RI sensing and can broaden the applications of nanophotonic sensors.

Data availability statement

All data that support the findings of this study are included within the article (and any supplementary files).

Conflict of interest

The authors declare no conflicts of interest.

Funding

This work is supported by National Natural Science Foundation of China (Nos. T2394480, T2394481, 12 404 427, 12 234 007, 12 321 161 645, and 12 221 004); National Key R&D Program of China (2023YFA1406900 and 2022YFA1404800); Science and Technology Commission of Shanghai Municipality (24YF2702400, 22 142 200 400, 21DZ1101500, 2019SHZDZ X01, and 23DZ2260100). J W was also supported by the China National Postdoctoral Program for Innovative Talents (BX20230079) and the China Postdoctoral Science Foundation (2023M740721).

Author contributions

Yuyang Xu 0009-0006-0534-8921
Formal analysis (equal), Investigation (equal), Methodology (equal), Visualization (equal), Writing – original draft (equal)

Shunben Wu
Investigation (equal), Methodology (equal), Visualization (equal)

Ang Jiang 0009-0002-2664-1298
Investigation (equal), Methodology (equal), Visualization (equal)

Xiaohan Liu
Formal analysis (supporting), Investigation (supporting), Methodology (supporting)

Jiajun Wang 0000-0002-7554-370X
Conceptualization (lead), Formal analysis (equal), Methodology (equal), Project administration (equal), Supervision (equal), Visualization (equal), Writing – review & editing (equal)

Lei Shi
Conceptualization (equal), Supervision (equal), Writing – review & editing (equal)

References

[1] Altug H, Sang-Hyun O, Maier S A and Homola J 2022 Advances and applications of nanophotonic biosensors *Nat. Nanotechnol.* **17** 5–16
[2] Haleem A, Javaid M, Singh R P, Suman R and Rab S 2021 Biosensors applications in medical field: a brief review *Sens. Int.* **2** 100100
[3] Liu W *et al* 2023 Surface plasmon resonance sensor composed of microstructured optical fibers for monitoring of external and internal environments in biological and environmental sensing *Res. Phys.* **47** 106365
[4] Bourgeois W, Romain A-C, Nicolas J and Stuetz R M 2003 The use of sensor arrays for environmental monitoring: interests and limitations *J. Environ. Monit.* **5** 852–60
[5] Qin J, Jiang S, Wang Z, Cheng X, Baojun Li, Shi Y, Tsai D P, Liu A Q, Huang W and Zhu W 2022 Metasurface micro/nano-optical sensors: principles and applications *ACS Nano* **16** 11598–618
[6] Luchansky M S and Bailey R C 2012 High-Q optical sensors for chemical and biological analysis *Anal. Chem.* **84** 793–821
[7] Tittl A, John-Herpin A, Leitis A, Arvelo E R and Altug H 2019 Metasurface-based molecular biosensing aided by artificial intelligence *Angew. Chem., Int. Ed.* **58** 14810–22
[8] Xu Y, Bai P, Zhou X, Akimov Y, Png C E, Ang L-K, Knoll W and Lin W 2019 Optical refractive index sensors with plasmonic and photonic structures: promising and inconvenient truth *Adv. Opt. Mater.* **7** 1801433
[9] Tseng M L, Jahani Y, Leitis A and Altug H 2020 Dielectric metasurfaces enabling advanced optical biosensors *ACS Photonics* **8** 47–60
[10] Wang Y, Sun C, Li H, Gong Q and Chen J 2017 Self-reference plasmonic sensors based on double Fano resonances *Nanoscale* **9** 11085–92
[11] Wang S, Liu Y, Zhao D, Yang H, Zhou W and Sun Y 2017 Optofluidic Fano resonance photonic crystal refractometric sensors *Appl. Phys. Lett.* **110** 091105
[12] Zhang Y, Liang Z, Meng D, Qin Z, Fan Y, Shi X, Smith D R and Hou E 2021 All-dielectric refractive index sensor based on Fano resonance with high sensitivity in the mid-infrared region *Res. Phys.* **24** 104129
[13] Rodrigo D *et al* 2018 Resolving molecule-specific information in dynamic lipid membrane processes with multi-resonant infrared metasurfaces *Nat. Commun.* **9** 2160
[14] Xiao S, Wang T, Liu Y, Han X and Yan X 2017 An ultrasensitive and multispectral refractive index sensor design based on quad-supercell metamaterials *Plasmonics* **12** 185–91
[15] Feng W, Liu D, Yan Li and Hongju Li 2022 Ultra-sensitive refractive index sensing enabled by a dramatic ellipsometric phase change at the band edge in a one-dimensional photonic crystal *Opt. Express* **30** 29030–43
[16] Zhang K, Chen Z, Hongju Li, Zao Y, Liu Y and Xiaohu W 2023 A dual-band hydrogen sensor based on Tamm plasmon polaritons *Phys. Chem. Chem. Phys.* **25** 20697–705
[17] Wang J *et al* 2024 Optical bound states in the continuum in periodic structures: mechanisms, effects and applications *Photon. Insights* **3** R01
[18] Shiyu Li, Zhou C, Liu T and Xiao S 2019 Symmetry-protected bound states in the continuum supported by all-dielectric metasurfaces *Phys. Rev. A* **100** 063803
[19] Huang L, Lei X, Powell D A, Padilla W J and Miroshnichenko A E 2023 Resonant leaky modes in all-dielectric metasystems: fundamentals and applications *Phys. Rep.* **1008** 1–66
[20] Romano S, Zito G, Torino S, Calafiore G, Penzo E, Coppola G, Cabrini S, Rendina I and Mocella V 2018 Label-free sensing of ultralow-weight molecules with all-dielectric metasurfaces supporting bound states in the continuum *Photon. Res.* **6** 726–33
[21] Liu Z, Guo T, Tan Q, Hu Z, Sun Y, Fan H, Zhang Z, Jin Y and He S 2023 Phase interrogation sensor based on all-dielectric BIC metasurface *Nano Lett.* **23** 10441–8
[22] Yesilkoy F, Arvelo E R, Jahani Y, Liu M, Tittl A, Cevher V, Kivshar Y and Altug H 2019 Ultrasensitive hyperspectral imaging and biodetection enabled by dielectric metasurfaces *Nat. Photon.* **13** 390–6
[23] Wang J, Kühne J, Karamanos T, Rockstuhl C, Maier S A and Tittl A 2021 All-dielectric crescent metasurface sensor driven by bound states in the continuum *Adv. Funct. Mater.* **31** 2104652
[24] Feng W, Qin M and Xiao S 2022 Quasi-bound state in the continuum supported by a compound grating waveguide structure for high-figure-of-merit refractive-index sensing *J. Appl. Phys.* **132** 193101
[25] Huang L, Shuangli Li, Zhou C, Zhong H, You S, Lin Li, Cheng Y and Miroshnichenko A E 2024 Realizing ultrahigh-Q resonances through harnessing symmetry-protected bound states in the continuum *Adv. Funct. Mater.* **34** 2309982
[26] Wenbin M and Zhou C 2023 Quasi-symmetry-protected BICs in a double-notched silicon nanodisk metasurface *Opt. Lett.* **48** 2158–61
[27] Huang L *et al* 2023 Ultrahigh-Q guided mode resonances in an all-dielectric metasurface *Nat. Commun.* **14** 3433
[28] Feng W, Liu D and Yu Xi 2023 Sensitive sucrose biosensors with high Q factors empowered by quasi-bound states in the continuum in compound grating waveguide structures *Res. Phys.* **49** 106539
[29] Luo M and Feng W 2024 Refractive-index sensing based on large negative Goos-Hänchen shifts of a wavy dielectric grating *Phys. Rev. Appl.* **22** 014050
[30] Romano S, Zito G, Lara Yépez S N, Cabrini S, Penzo E, Coppola G, Rendina I and Mocellaark V 2019 Tuning the exponential sensitivity of a bound-state-in-continuum optical sensor *Opt. Express* **27** 18776–86
[31] Jiaxin Lv, Chen Z, Yin X, Zhang Z, Weiwei H and Peng C 2020 High-sensitive refractive index sensing enabled by topological charge evolution *IEEE Photon. J.* **12** 1–10
[32] Luo M *et al* 2024 High-sensitivity optical sensors empowered by quasi-bound states in the continuum in a hybrid metal–dielectric metasurface *ACS Nano* **18** 6477–86
[33] Wang T, Liu S, Zhang J, Liang X, Yang M, Ding M, Jiang S, Jiao Q and Tan X 2024 Dual high-Q Fano resonances metasurfaces excited by asymmetric dielectric rods for refractive index sensing *Nanophotonics* **13** 463–75
[34] Cai Z, Zhiwei Li, Ravaine S, Mingxin H, Song Y, Yin Y, Zheng H, Teng J and Zhang A O 2021 From colloidal

particles to photonic crystals: advances in self-assembly and their emerging applications *Chem. Soc. Rev.* **50** 5898–951
[35] Galisteo-López J F, Ibisate M, Sapienza R, Froufe-Pérez L S, Blanco Alvaro and López C 2011 Self-assembled photonic structures *Adv. Mater.* **23** 30–69
[36] Liu J, Zhang X, Wenqing Li, Jiang C, Wang Z and Xiao X 2020 Recent progress in periodic patterning fabricated by self-assembly of colloidal spheres for optical applications *Sci. China Mater.* **63** 1418–37
[37] Yue Li, Cai W and Duan G 2008 Ordered micro/nanostructured arrays based on the monolayer colloidal crystals *Chem. Mater.* **20** 615–24
[38] Romanov S G, Korovin A V, Regensburger A and Peschel U 2011 Hybrid colloidal plasmonic-photonic crystals *Adv. Mater.* **23** 2515–33
[39] Shi L *et al* 2014 Coherent fluorescence emission by using hybrid photonic–plasmonic crystals *Laser Photon. Rev.* **8** 717–25
[40] Galisteo-López J F, López-García M, López C and García-Martín A 2011 Intrinsic losses in self-assembled hybrid metallodielectric systems *Appl. Phys. Lett.* **99** 083302
[41] López-García M, Galisteo-López J F, Blanco Alvaro, López C and García-Martín A 2010 High degree of optical tunability of self-assembled photonic-plasmonic crystals by filling fraction modification *Adv. Funct. Mater.* **20** 4338–43
[42] Zhou Y, Zheng H, Kravchenko I I and Valentine J 2020 Flat optics for image differentiation *Nat. Photon.* **14** 316–23
[43] Zhang W, Chu J, Deng R, Wang X, Tongyu Li, Liu W, Wang J, Liu X and Shi L 2024 Optical vortices generation via a self-assembly photonic crystal slab *Adv. Opt. Mater.* **12** 2400088
[44] Fan S, Suh W and Joannopoulos J D 2003 Temporal coupled-mode theory for the Fano resonance in optical resonators *J. Opt. Soc. Am. A* **20** 569–72
[45] Wang J, Zhao M, Liu W, Guan F, Liu X, Shi L, Chan C T and Jian Z 2021 Shifting beams at normal incidence via controlling momentum-space geometric phases *Nat. Commun.* **12** 6046
[46] Wang B, Liu W, Zhao M, Wang J, Zhang Y, Chen A, Guan F, Liu X, Shi L and Jian Z 2020 Generating optical vortex beams by momentum-space polarization vortices centred at bound states in the continuum *Nat. Photon.* **14** 623–8
[47] Liu W, Shi L, Jian Z and Chan C T 2021 Ways to achieve efficient non-local vortex beam generation *Nanophotonics* **10** 4297–304
[48] Zhang Y *et al* 2021 Momentum-space imaging spectroscopy for the study of nanophotonic materials *Sci. Bull.* **66** 824–38
[49] Haynes W M 2016 *CRC Handbook of Chemistry and Physics* (CRC Press)